

Electronic Supplementary Material (ESI) for Soft Matter.

This journal is © The Royal Society of Chemistry 2020

Supporting Information

Polypyrrole and polyaniline nanocomposites with high photothermal conversion efficiency

Lorena Ruiz-Perez,^{a,b,†} Loris Rizzello,^{a,c,†} Jinping Wang,^{d,e} Nan Li,^d Giuseppe Battaglia,^{*a,b,f}
Yiwen Pei^{*a,g}

^aDepartment of Chemistry, University College London, London, WC1H 0AJ, UK

^bThe EPSRC/JEOL Centre for Liquid Electron Microscopy, London, WC1H 0AJ, UK

^cPresent addresses: 1) Department of Pharmaceutical Sciences, University of Milan, via Mangiagalli 25, 20133, Milano, Italy; 2) Institute for Bioengineering of Catalonia (IBEC), The Barcelona Institute of Science and Technology, C/ Baldiri Reixac, 15-21 · 08028 Barcelona, Spain

^dTianjin Key Laboratory of Drug Delivery & High-Efficiency, School of Pharmaceutical Science and Technology, Tianjin University, 300072, PR China.

^ePresent address: Department of Biomedical Engineering, Stevens Institute of Technology, Hoboken, New Jersey 07030, United States.

^fDepartment of Chemical Engineering, University College London, London, UK

^gPresent address: Chemical and Biological Sciences, National Physical Laboratory, London, TW11 0LW, UK

[†] L.R-P. and L.R. contributed equally to this work as first authors

Methods

Materials. All chemicals were purchased from the Sigma-Aldrich Chemical Company and used as received unless otherwise noted. 2-Hydroxypropyl methacrylate (HPMA) was purchased from Aldrich and contains an isomeric mixture of 75 mol% HPMA and 25 mol% 2-hydroxyisopropyl methacrylate. Cyanine5 amine (Cy5 amine) was purchased from Lumiprobe Chemical Company. Semi-permeable cellulose tubing was purchased from SPECTRA/POR (molecular weight cut-off is 1000 Da).

RAFT Polymerisation-induced Self-Assembly. Poly[2-(Methacryloyloxy)ethyl phosphorylcholine] (PMPC) homopolymer and PMPC-PHPMA diblock copolymers were synthesized by RAFT according to a literature protocol.¹ Briefly, 4,4-azobis(4-cyanovaleric acid) (V-501) (22.8 mg, 0.08 mmol) and 4-cyanopentanoic acid dithiobenzoate (CPADB) (113 mg, 0.406 mmol) were firstly dissolved in 5 wt% sodium bicarbonate aqueous solution. A solution of MPC (3 g, 10.2 mmol) in Milli-Q water (15.6 g) was then added to the reaction mixture. The solution was purged with nitrogen for 40 min and then placed in a pre-heated oil bath at 70 °C for 2 h under continuous stirring. At the end of the polymerisation, the reaction was ceased via rapid cooling in an ice/water bath and exposure to air. The crude product was subject to ¹H NMR analysis to calculate monomer conversion and was then purified by dialysis against Milli-Q water. The final pure product was obtained by lyophilisation. In a general RAFT PISA formulations of diblock copolymer synthesis at 10 wt% total solids, a solution of PMPC₄₃ (0.1 g, 0.008 mmol), V-501 (0.7 mg, 0.003 mol) and HPMA (0.65 g, 4.5 mmol) in Milli-Q water (6.8 g) was degassed under nitrogen for 40 min before placing in a pre-heated oil bath at 70 °C for 24 h under continuous stirring. At the end of the reaction, the polymerisation was quenched via rapid cooling in an ice/water bath and exposure to air. The crude product (0.1 mL) was collected and subject to ¹H NMR analysis to calculate monomer conversion.

Synthesis of Conjugated Polymer Nanoparticles. A general procedure for the synthesis of polypyrrole micelles via chemical oxidation is as follows. A solution containing iron(III) chloride (18.7 mg, 0.12 mmol) and a diluted aqueous dispersion of PMPC₄₃-*b*-PHMPA₂₅₈ (1 mL, 0.7 wt% total solids) was added to a reaction vessel equipped with a magnetic stir bar. The reaction vessel was sealed and the solution was stirred or sonicated either at 25°C or at 0

°C for 1 h. Subsequently, pyrrole (3.4 mg, 0.05 mmol) was slowly added to the reaction mixture and the solution was continuously stirred or sonicated either at room temperature or at 0 °C for 4 h. At the end of the reaction, the resulting nanoparticles were purified by dialysis against Milli-Q water. Syntheses of polypyrrole vesicles, polyaniline micelles and vesicles were performed in a similar fashion.

Functionalisation of Conjugated Polymer Particles with Fluorescent Dye Cy5.

Polypyrrole Micelles (7 mg) was dispersed in 1 mL PBS buffer solution (pH 5, adjusted using 1 M HCl) in a 10 mL round bottom flask, followed by the addition of 1-ethyl-3-(3-dimethylaminopropyl) carbodiimide (EDC, 2.0 mg, 1.04×10^{-5} mol) and N-hydroxysuccinimide (NHS, 4.0 mg, 3.47×10^{-5} mol). The reaction mixture was stirred for 5 min at ambient temperature. Cyanine5 amine (Cy5 amine, 1.0 mg, 1.53×10^{-6} mol) was then added to the reaction flask and the reaction mixture was stirred overnight at ambient temperature. At the end of the reaction, the functionalised particles were purified through dialysis against water for 2 days.

Dynamic light scattering. The average particle size in the PPy and PANI dispersions was determined by dynamic light scattering using a Malvern Instrument Zetasizer Nano Series instrument. The scattered light was detected at an angle of 173°. For sample preparation, all dispersions were diluted to minimize the interaction between the nanoparticles.

UV-vis absorption. The absorption spectra of the PPy and PANI dispersions were recorded using a Perkin Elmer Lambda 25 UV-vis spectrometer. For sample preparation, all the polymer dispersions were diluted with Milli-Q water. pH-responsive PANi micelles were diluted either with water (pH neutral) or with acidic water (pH 4) before the measurement.

Fourier transform infrared (FTIR) spectroscopy. FTIR spectroscopy was conducted on a Bruker IFS 66/S instrument under attenuated total reflectance (ATR). An average of 64 scans were performed on each sample. The results were analyzed using OPUS software version 4.0.

Nuclear Magnetic Resonance (NMR) spectroscopy. NMR spectroscopic measurements were conducted on a Bruker DPX 300 instrument at 300 MHz for hydrogen nuclei. The

internal solvent signal of D₂O (δ (D₂O) = 4.79 ppm) was used as reference. ¹³C solid-state NMR was performed on the freeze-dried samples of PPy and PANI micelles. Magic-angle spinning (MAS) spectra were acquired on a Bruker ASCEND (300 MHz) spectrometer. The measurement was performed utilizing 8 kHz MAS, a 1 s recycle delay, 23k scans and a 1 ms ramped cross polarization time at 25 °C.

Photothermal performance. Thermal images were captured by an SC300 infrared camera (Fluke TiR, USA) and analyzed by Examin IR image software (FLIR). The excitation source was an 808 nm diode-pumped continuous-wave solid-state laser system (LASERGLOW Technologies, Shanghai, China).

To measure the photothermal performances of the samples, an 808 nm NIR laser was employed to deliver perpendicular through a quartz cuvette containing aqueous dispersion (0.5 mL) of the sample with concentration of 0.2 mg mL⁻¹ or 1.0 mg mL⁻¹. Water was used as a control. The NIR laser light source was equipped with a power of 1.5 W cm⁻² under the 808 nm semiconductor laser device with a 5 mm diameter laser module. The temperature was measured using a thermocouple thermometer that was inserted into the aqueous dispersion perpendicular to the path of the laser light.

The photothermal conversion efficiency of the sample was determined according to the reported method.^{2,3} To measure the photothermal conversion efficiency (η), the aqueous dispersion samples were exposed to 808 nm NIR laser (1.5 W cm⁻²) for 600 s, and then the laser was shut off. The heating and cooling temperature trends of samples were recorded by temperature gauge. The photothermal conversion efficiency was calculated according to the eq 1:

$$\eta = \frac{hS(T_{max} - T_{Surr}) - Q_0}{I(1 - 10^{-A808})} \quad (1)$$

Where h is the heat transfer coefficient, S is the sample container surface area, T_{max} is the steady state maximum temperature, T_{surr} is the ambient room temperature, Q_0 is the baseline

energy input by the solvent and the sample container without NPs, I is the laser power, and A_{808} is the absorbance of NPs at 808 nm.

In order to get the hS , θ herein is introduced, which is defined as the ratio of $(T - T_{surr})$ to $(T_{Max} - T_{surr})$:

$$\theta = \frac{T - T_{surr}}{T_{Max} - T_{surr}} \quad (2)$$

Thus, the value of hS is calculated by eq 3:

$$\tau_s = \frac{C_d m_d}{hS} \quad (3)$$

Where τ_s is the characteristic thermal time constant, the mass of the nanoparticle solution (m_d) is g, and its heat capacity (C_d) is approximately $4.2 \text{ J g}^{-1} \text{ K}^{-1}$ (the heat capacity of water). The heat energy (Q_0) of the sample container and solvent without nanoparticles is referred to a literature value ($Q_0 = 3.5 \text{ J}$) described elsewhere.^{2,3}

Transmission Electron Microscopy (TEM) imaging. Conventional and Energy filtered-TEM (EFTEM) imaging were performed using a JEOL JEM-2200FS TEM equipped with a field emission gun (FEG) at 200 kV, and an in-column Omega filter. Images were taken at a collection angle of 24.282 mrad and in parallel imaging conditions for TEM mode. The STEM mode image was taken under convergent beam conditions. Image J was used to measure the TEM-measured number averaged diameter of both the templates and the CP-based nanoparticles. Twenty nanoparticles were measured for each formulation taken from different areas of the grid and different batches to allow for good statistics.

The block copolymer templates, PMPC₄₃-*b*-HPMA₂₅₈ and PMPC₁₅-HPMA₄₄₅, were stained using a phosphotungstic acid (PTA) solution at 0.75 wt%. The solution was prepared by dissolving 37.5 mg of PTA in boiling distilled water (5 mL). The pH was adjusted to 7.0 by adding a few drops of 5 M NaOH under continuous stirring. The PTA solution was then filtered through a 0.2 μm filter. Copper grids were glow-discharged for 40 seconds in order to render them hydrophilic. Then 5 μL of sample (concentration = 0.5 mg mL^{-1}) was deposited

onto the grids for one minute. After that, the grids were blotted with filter paper and immersed into the PTA staining solution for 3 seconds for negative staining. Then the grids were blotted again and dried under vacuum for 1 minute. Fe^{3+} complexed PMPC₁₅-HPMA₄₄₅ vesicles and all the CP-based nanoparticles were imaged in absence of PTA staining.

Elemental analysis of the specimens was performed using the microscope in energy-filtered transmission electron microscopy (EF-TEM) mode with the aim to obtain fine structure imaging. The software used for image acquisition and processing was the Digital Micrograph™ software (version 3.20). Images were recorded using a charge coupled device (CCD) camera US1000XP from Gatan.

In EF-TEM mode, chemical mapping was achieved by selecting electrons that have lost a specific amount of energy from inelastic scattering. In the case of inner shell ionization, the energy loss is characteristic of the element the electron interacted with in the specimen. In the present study the elements investigated were Iron and Phosphorus. Conventional unfiltered TEM images and Iron/phosphorus maps were acquired. For the elemental maps electrons were collected post specimen and dispersed using the Omega filter. An electron energy loss spectrum (EELS) was traced across the dispersion plane. From the spectrum the region of interest was selected with an energy window; the subsequent insertion of an energy slit allowed for the image to be formed.

The Iron present in the structures was identified by exciting the atomic M shell with a slit width of 3 eV. The Iron ionisation energy in the M_{2,3} edges is 54 eV. The Phosphorus element present in the imaged structures was identifying by exciting the atomic L shell with a slit of 10 eV. The Phosphorus ionisation energy in the L_{2,3} edges is 132 eV. The 3-window technique was employed. This technique involves acquiring two images before and one after the ionization edge. The pre-edge images are used to compute the approximate background contained in the post-edge window. Once the background is determined and removed, the subsequent map displays a signal that is proportional to the element concentration in the sample. The first pre-edge, second pre-edge, and post-edge energies were 47.5 eV, 50.5 eV, and 55.5 eV respectively for Iron mapping. The first pre-edge, second pre-edge, and post-edge energies were 115 eV, 125 eV, and 137 eV respectively for Phosphorus mapping. The elastic

TEM image and the false colour chemical mapping were superimposed using ImageJ software.

Relative thickness maps were also obtained in the EF-TEM technique by acquiring an unfiltered and zero-loss image from the same region under identical conditions. Thickness maps evaluate the sample local thickness in terms of electron mean free path (mfp). Electron mean free paths values between 1 and 2 represent the best sample thickness conditions for performing efficient elemental mapping.

Cell cultures, metabolic assays and confocal imaging. HeLa cells were cultured and maintained using DMEM containing: 10 (v/v) fetal calf serum, 2 mM L-glutamine, 100 mg/ml streptomycin and 100 IU/ml penicillin. Cells were cultured at 37 °C/95% air/5% CO₂. Cells were periodically sub-cultured using Trypsin-EDTA solution 0.25% for the detachment process and centrifuged at 2000 rpm for 5 minutes for the pellet collection. THP-1 were cultured and maintained in RPMI-1640 medium, supplemented with 10 mM HEPES buffer, and 10 (v/v) fetal calf serum, 2 mM L-glutamine, 100 mg/ml streptomycin and 100 IU/ml penicillin. THP-1 monocytes were differentiated to macrophages through incubation with 5 ng/mL of PMA for 48 hours.⁴ We chose this PMA concentration as it has been found to not undesirable regulate genes expression.⁵

For metabolic assay, the MTT method was used. Briefly, cells were seeded at a concentration of 5×10^3 cells/well in a 96 well plate overnight. Increasing concentrations of nanoparticles were then added in the growth media, namely 1, 0.2, 0.1, 0.02 mg mL⁻¹, for 24 and 48 hours. The medium growth was then removed, and the Tetrazolium Blue salt added for 2 hours. An acidified solution of isopropanol was then added to dissolve the water-insoluble MTT formazan. The solubilized blue crystals were measured colorimetrically at 570 nm (plate reader ELx800, BioTek).

For uptake imaging analyses, HeLa and THP-1 cells were seeded on glass-bottom petri dishes (Ibidi) at a concentration of 5×10^3 cells/well, and incubated with Cy5-labeled nanoparticles (0.1 mg mL⁻¹) for 24 and 48 hours, followed by 3 steps of PBS washing. Cells were then stained with DAPI for nuclear staining, and imaged with confocal microscope (Leica SP8). For the

uptake quantification, 10 different regions of the petri dishes were captured, and the fluorescent signal has been normalized to the nuclear intensity signal (using ImageJ).

Particle formation: using the PISA-made micellar PMPC₄₃-PHPMA₂₅₈ templates, monodisperse PPy- and PANI-based nanoparticles can be successfully produced with TEM-measured number-average diameters of (98 ± 10) nm and (100 ± 12) nm, respectively. The TEM measurements are in good agreement of the DLS-measured hydrodynamic diameters of 192.3 nm ($\mu_2/I^2 = 0.21$) and 126.8 nm ($\mu_2/I^2 = 0.24$). The use of vesicular PMPC₁₅-PHPMA₄₄₅ templates allows the successful formation of PPy- and PANI-based vesicles whose TEM-measured diameters of (118 ± 11) nm and (101 ± 8) nm and DLS-determined sizes of 190.1 nm ($\mu_2/I^2 = 0.23$) and 360.2 nm ($\mu_2/I^2 = 0.19$). The discrepancy between TEM and DLS results in PANI vesicles suggests certain degree of agglomerations during the particle formation (Table S1).

Table S1. Summary of the nanoparticle compositions, the observed TEM morphology, the DLS-measured number-average hydrodynamic diameter (D_h) and polydispersities (μ_2/T^2). All the block copolymer compositions were measured by ¹H NMR.

Entry	Compositions	TEM morphology	DLS	
			D_h (nm)	μ_2/T^2
1	PMPC ₄₃ -PHPMA ₂₅₈	Micelles	103.4	0.03
2	PPy-based PMPC ₄₃ -PHPMA ₂₅₈	Micelles	192.3	0.21
3	PANI-based PMPC ₄₃ -PHPMA ₂₅₈	Micelles	126.8	0.24
4	PMPC ₁₅ -PHPMA ₄₄₅	Vesicles	122.4	0.03
5	PPy-based PMPC ₁₅ -PHPMA ₄₄₅	Vesicles	190.1	0.23
6	PANI-based PMPC ₁₅ -PHPMA ₄₄₅	Vesicles	360.2	0.19

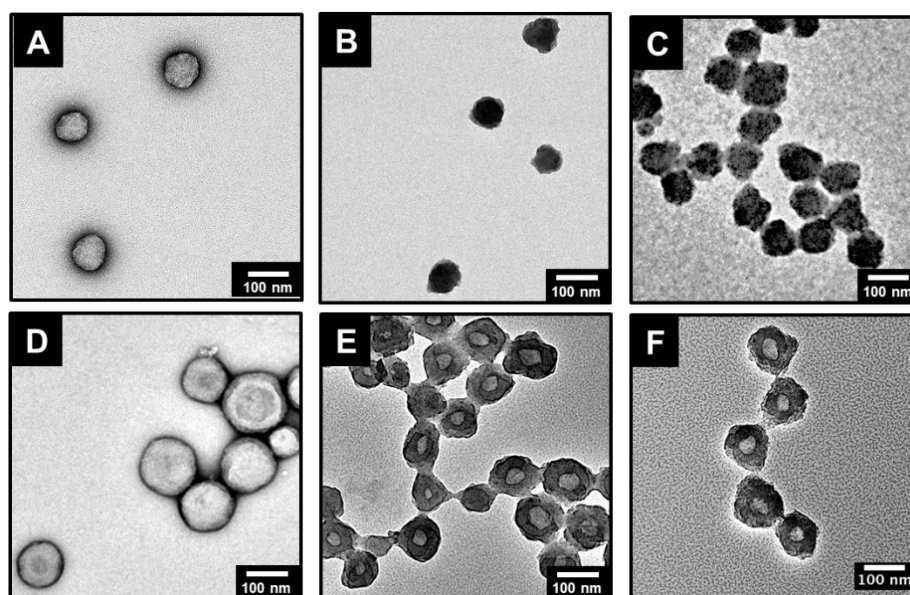


Figure S1. Conventional TEM micrographs of (A) PTA stained PMPC₄₃-HPMA₂₅₈ template structures showing sphere formation, (B) PPy- and (C) PANI-based PMPC₄₃-PHPMA₂₅₈ micelles; (D) PTA-stained PMPC₁₅-HPMA₄₄₅ template structures showing formation of vesicles, (E) PPy- and (F) PANI-based PMPC₁₅-HPMA₄₄₅ vesicles.

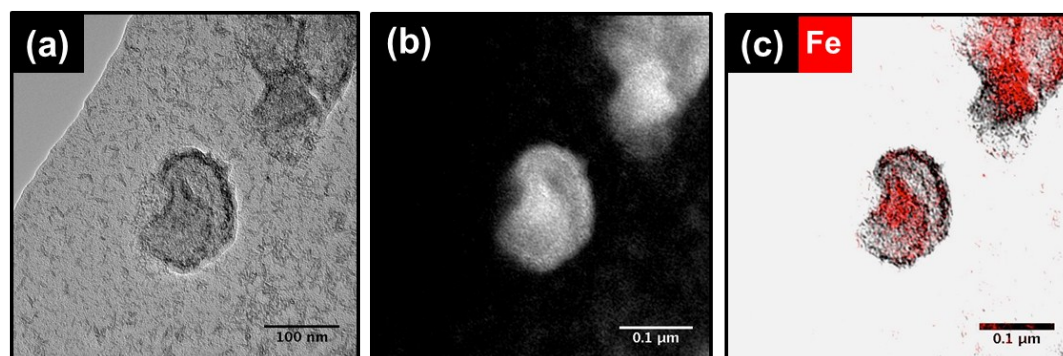


Figure S2. Energy filtered TEM micrographs displaying **a**, zero-loss elastic image and **b**, thickness map of the Fe³⁺-complexed PMPC₁₅-HPMA₄₄₅ vesicles; **c**, Fe elemental map (red signal) superimposed to zero-loss image shown in **a**.

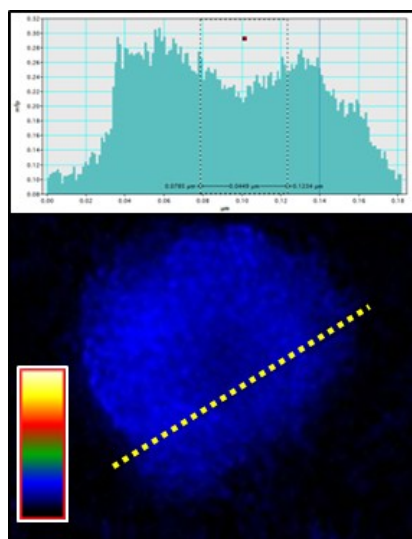
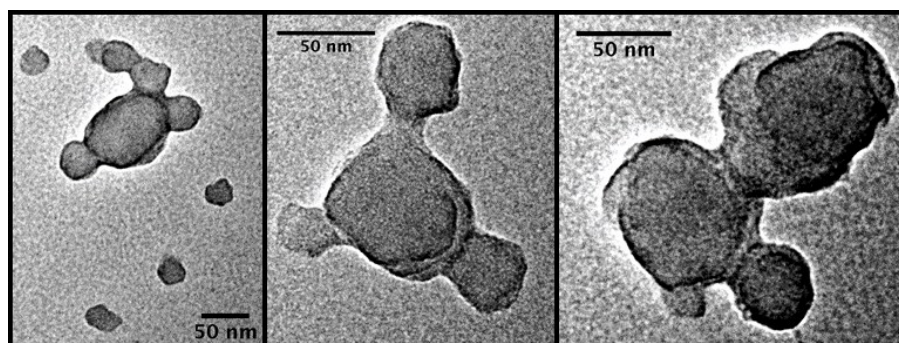


Figure S3. False colored thickness map of the Fe^{3+} -complexed PMPC_{15} - PHPMA_{445} vesicles, in the absence of any conducting polymer, displaying electron mean free path (mfp) color scale on the bottom right. Blue corresponds to mfp value of circa 1 indicating appropriate thickness for optimal elemental mapping. Inset top image: thickness profile across vesicle shows a thinner region in the core mirroring vesicular structures.

Optimization of reaction conditions: Various mixing methods and reaction conditions have been performed to optimize the fabrication of CP-based colloids. To investigate the effect of iron/PHPMA complexation on the formation of PPy micelles, the $[\text{FeCl}_3]/[\text{OH}]$ (the hydroxyl group in PHPMA) molar ratio was varied from 0.5 to 10.4 with a fixed $[\text{FeCl}_3]/[\text{pyrrole}]$ molar ratio of 2.3. As shown in Table S2 and Fig. S4, a clear dependence of particle size and morphologies was observed by transmission electron microscopy (TEM) and dynamic light scattering (DLS) analysis. For systems using PMPC-PHPMA spherical templates, an optimized $[\text{FeCl}_3]/[\text{OH}]$ molar ratio of 3.2 was found to produce uniform PPy micelles. At higher molar ratio, the formation of PPy also appeared on the particle surfaces. Further increase of this ratio leads to the formation of a macroscopic black precipitate consistent with the limited solubility features of PPy in water and the absence of the PMPC chains as a stabilising block. At low molar ratio, however, yellow milky dispersions were observed. This clearly suggests that there is little, or no, formation of PPy, but more likely oligopyrrole, under these conditions. Intriguingly, large variations in colloidal stability could be found when the post-PISA reaction temperature and the mixing method were varied. Lowering the temperature to *approx.* 0 °C or mixing the reaction ultrasonically during post-PISA treatment results in large agglomerations – indication of the promise of this fabrication approach to produce CP at different length scale.

Table S2. Effect of reaction conditions during the post-PISA treatment on the formation of the CP-based micelles. The observed morphology and stability of CP-based particles depend on the molar ratio of $[\text{Fe}^{3+}]/[\text{OH}^-]$, mixing methods and reaction temperature.

Entry	Molar ratio $[\text{Fe}^{3+}]/[\text{OH}^-]$	Mixing methods	Reaction temperature	Comments
1	10.4	stirred	25°C	Macroscopic black precipitates
2	6.4	stirred	25°C	Sterically stable, black suspension containing small clusters
3	3.2	stirred	25°C	Uniform and sterically stable black suspension
4	1.0	stirred	25°C	Dark yellow milky suspension
5	0.5	stirred	25°C	Light yellow milky suspension
6	3.2	stirred	0°C	Macroscopic black precipitates
7	3.2	sonicated	25°C	Macroscopic black precipitates

**Figure S4.** The TEM images of the PPy-based particles using a $[\text{Fe}^{3+}]/[\text{OH}^-]$ molar ratio of 6.4. It is observed that the formation of PPy clusters consist of several micelles.

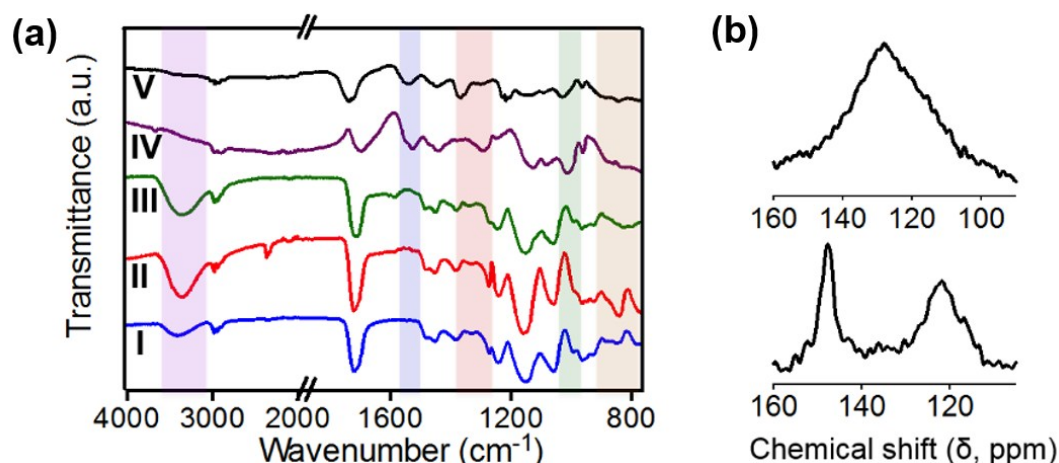


Figure S5. **a)** FT-IR spectra of unmodified PMPC-PHPMA particles (I), PANI- and PPy-based micelles (II, IV) and vesicles (III, V) suspension. **b)** ¹³C NMR spectra of PPy (top)- and PANI-based (bottom) particles.

In the FTIR spectra of PPy particles, the bands found at 1550 cm⁻¹, 1350 cm⁻¹, 1005 cm⁻¹ and 950 cm⁻¹ are likely attributed to stretching vibration of C=C units, C-N absorption, and =C-N in-plane and out-plane deformation vibration, respectively (Fig. 5Sa).⁶ For PANI particles, the characteristic peaks at 3390 cm⁻¹, 3020 cm⁻¹, 1590 cm⁻¹, 1290 cm⁻¹ 830 cm⁻¹ correspond to the N-H stretching vibration, aromatic C-H stretching, benzene/quinone ring deformation, C=N stretching of a secondary aromatic amine, and aromatic C-H out-of-plane bending.⁷ In Fig. 5Sb, high-resolution solid-state ¹³C NMR shows the characteristic carbon resonance of *c.a.* 125 ppm which is associated with α - α' linkages of PPy⁸ while two peaks at *c.a.* 120 ppm and *c.a.* 158 ppm were likely linked to C-C linkages and C=N quinoid resonance of PANI.⁹

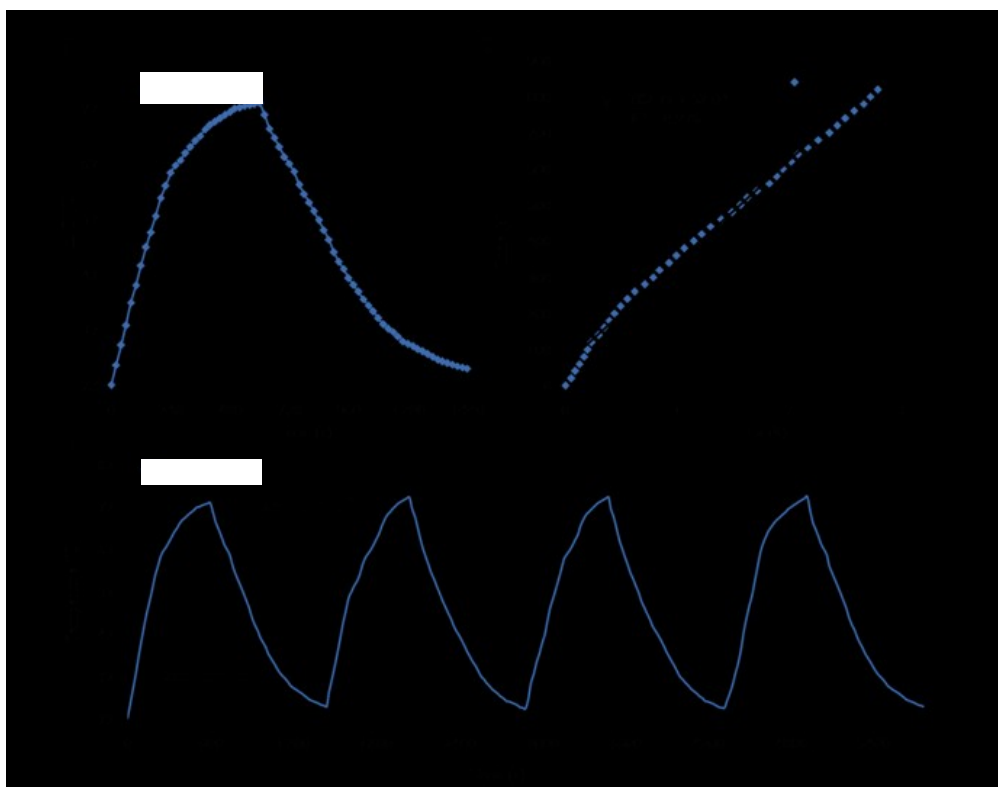


Figure S6. (a) Representative photothermal effect of the irradiation of the aqueous dispersion of PPy-based nano-vesicles (0.2 mg ml^{-1}) with the NIR laser (808 nm , 1.5 Wcm^{-2}). The irradiation lasted for 10 min, and then the laser was turned off. (b) Plot of cooling time *versus* negative natural logarithm of the temperature driving force that is obtained from the cooling stage. (c) Temperature monitoring of the CP-based dispersion during the successive cycles of an on-and-off laser. The photothermal conversion efficiency (η) is 24.2%.

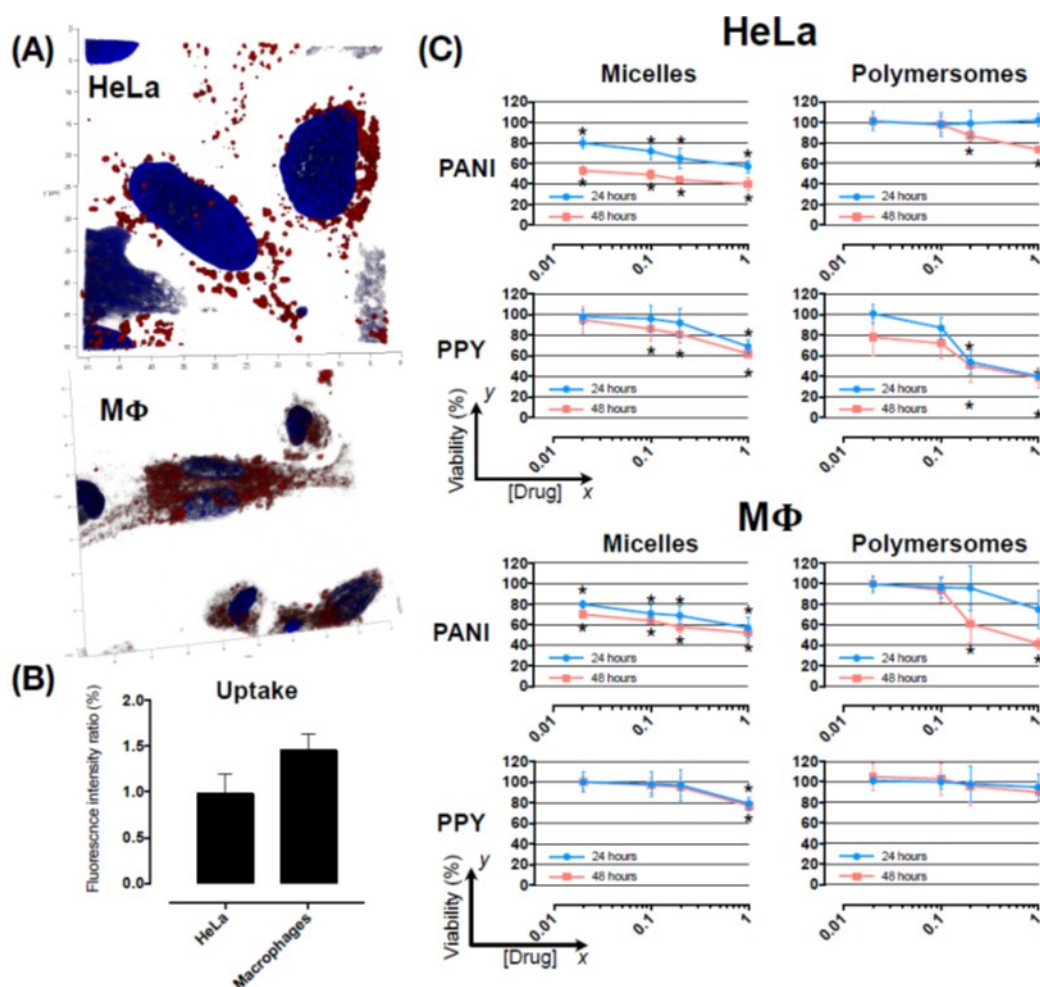


Figure S7. Interactions of CP-based nanoparticles with cells. **A**, 3D-confocal microscopy for uptake imaging using dye-functionalised PPy micelles. **B**, Quantification of uptake. **C**, Cell metabolic assay (MTT) for PANI and PPY micelles and vesicles (also known as polymersomes). Concentration tested: 1, 0.2, 0.1, 0.02 mg mL⁻¹. $n = 3$ independent experiments. Statistic: t -test with $*p < 0.05$ compared to untreated cells.

Cytotoxicity studies show that PANI micelles possess a concentration-dependent toxicity in HeLa after 48 hours, while the PPy micelles slightly affected the cell metabolic activity only at the highest concentration tested. Furthermore, all the CP vesicles were highly tolerated by in HeLa after 24 hours of incubation time, with a moderate decrease in cell viability detected after 48 hours, only for the highest concentrations tested. The results described for the HeLa cells follow a similar trend in MΦ.

References:

- [1] S. Sugihara; A. Blanz; S. P. Armes; A. J. Ryan; A. L. Lewis. *J. Am. Chem. Soc.* 2011, 133, 15707-15713.
- [2] Q. Tian; J. Hu; Y. Zhu; R. Zou; Z. Chen; S. Yang; R. Li; Q. Su; Y. Han; X. Liu. *J. Am. Chem. Soc.* 2013, 135, 8571-8577.
- [3] C. Ayala-Orozco; C. Urban; M. W. Knight; A. S. Urban; O. Neumann; S. W. Bishnoi; S. Mukherjee; A. M. Goodman; H. Charron; T. Mitchell; M. Shea; R. Roy; S. Nanda; R. Schiff; N. J. Halas; A. Joshi. *ACS Nano* 2014, 8, 6372-6381.
- [4] M. Daigneault; J. A. Preston; H. M. Marriott; M. K. B. Whyte; D. H. Dockrell. *PLoS one* 2010, 5, e8668.
- [5] E. K. Park; H. S. Jung; H. I. Yang; M. C. Yoo; C. Kim; K. S. Kim. *Inflamm. Res.* 2007, 56, 45-50.
- [6] H. P. de Oliveira, C. A. S. Andrade and C. P. de Melo, *J. Colloid Interface Sci*, 2008, 319, 441-449.
- [7] R. Panigrahi and S. K. Srivastava, *RSC Adv.*, 2013, 3, 7808-7815.
- [8] M. Forsyth, V.-T. Truong and M. E. Smith, *Polymer*, 1994, 35, 1593-1601.
- [9] A. Yasuda and T. Shimidzu, *Synthetic metals*, 1993, 61, 239-245.